Supplementary Material

Fabrication of a novel separation-free heterostructured photocatalyst with enhanced visible light activity in photocatalytic degradation of antibiotics

Xingkui Guo[a], Fan Yang[a,*], Xiaolu Sun[a], Chuang Han[a], Yujiao, Bai[a], Guanjun Liu[a], Wenbo Liu[a], Rongguo Wang [a,b,*]

[a] National Key Laboratory of Science and Technology on Advanced Composites in Special Environments
Harbin Institute of Technology
Harbin 150080, P. R. China
[b] Shenzhen STRONG Advanced Materials Research Institute Co., Ltd
Shenzhen, P. R. China

E-mail: wrg@hit.edu.cn; yngfan@163.com

Supplementary material:

Figure captions

Fig. S1. SEM image (a), EDS (c), TEM image (c) and HRTEM image (d) of PDMAA-TiO_2 hydrogel; SEM image (e), EDS (f), TEM image (g) and HRTEM image (h) of PDMAA-CuS hydrogel.

Fig. S2. a) UV-vis diffuse reflectance spectra of TiO_2 particles, CuS particles, PDMAA-TiO_2, PDMAA-CuS and PDMAA-TiO_2/CuS hydrogel. b) The band gap evaluation for linear dependence of $(Ahv)^2$ versus hv for TiO_2 and CuS.

Fig. S3. a) Photoluminescence spectra of PDMAA-TiO_2, PDMAA-CuS and PDMAA-TiO_2/CuS hydrogel. b) The transient photocurrent response of PDMAA-TiO_2, PDMAA-CuS and PDMAA-TiO_2/CuS photocatalyst electrodes with light on-off cycles under visible light irradiation.

Fig. S4. TGA curves of PDMAA, PDMAA-TiO_2, PDMAA-CuS, and PDMAA-TiO_2/CuS hydrogels.

Fig. S5. The swelling ratio of PDMAA-TiO_2, PDMAA-CuS and PDMAA-TiO_2/CuS hydrogel.

Fig. S6. Zeta potentials of PDMAA, PDMAA-TiO_2, PDMAA-CuS and PDMAA-TiO_2/CuS hydrogel.

Fig. S7. FTIR spectra (a) PDMAA, (b) PDMAA-TiO_2 and (c) PDMAA-TiO_2/CuS hydrogel.

Fig. S8. XRD spectra of TiO_2 nanoparticle, and PDMAA, PDMAA-TiO_2, PDMAA-

CuS and PDMAA-TiO_2/CuS hydrogel.

Fig. S9. a) Adsorption isotherm analyses of sulfaclozine on PDMAA-TiO_2/CuS hydrogel. Conditions: hydrogel 0.1g, pH_0= 7.0, 25 °C. b) Adsorption isotherm analyses with Langmuir model of sulfaclozine on PDMAA-TiO_2/CuS hydrogel. Conditions: hydrogel 0.1g, pH_0= 7.0, 25 °C.

Fig. S10. High-resolution XPS spectra (a) N 1s, (b) O 1s, (c) S 2p, (d) Ti 2p of PDMAA-TiO_2 hydrogel before and after the adsorption of sulfaclozine.

Fig. S11. High-resolution XPS spectra (a) N 1s, (b) O 1s, (c) S 2p, (d) Cu 2p of PDMAA-CuS hydrogel before and after the adsorption of sulfaclozine.

Fig. S12. High-resolution XPS spectra of (a) Ti 2p and (b) O 1s for PDMAA-TiO2, (c) S 2p and (d) Cu 2p for PDMAA-CuS, and (e) Ti 2p, (f) O 1s, (g) S 2p, and (h) Cu 2p for PDMAA-TiO2/CuS composite.

Fig. S13. The photodegradation rate of sulfaclozine using PDMAA-TiO_2, PDMAA-CuS, PDMAA-TiO_2/CuS hydrogel, and mix (PDMAA-CuS hydrogel and TiO_2 nanoparticles) with 300W visible light.

Fig. 14. The MS data and proposed structures of the intermediates of sulfaclozine photodegradation in the composite hydrogel catalysis system.

Fig. S15. The TOC removal ratio of sulfaclozine in the composite hydrogel catalysis system.

Fig. S16. The curves of the removal rate for sulfaclozine using PDMAA-TiO_2/CuS hydrogels at various circumstances including adsorption before degradation, adsorption

again after degradation, and repeating adsorption without degradation.

Fig. S17. XRD spectra of PDMAA-TiO_2/CuS hydrogel before and after the cycling test.

Fig. S18. XPS spectra of PDMAA-TiO_2/CuS hydrogel before and after the cycling test.

Fig. S19. The SEM images of PDMAA-TiO_2/CuS hydrogel (a) before and (b) after the cycling test.

Fig. S20. The TEM images of PDMAA-TiO_2/CuS hydrogel (a,b,c) before and (d, e, f) after the cycling test.

Table S1. The photodegradation intermediates of sulfaclozine.

Table S2. Property comparison of photocatalysts reported in recent three years for degradation of antibiotics under visible light irradiation.

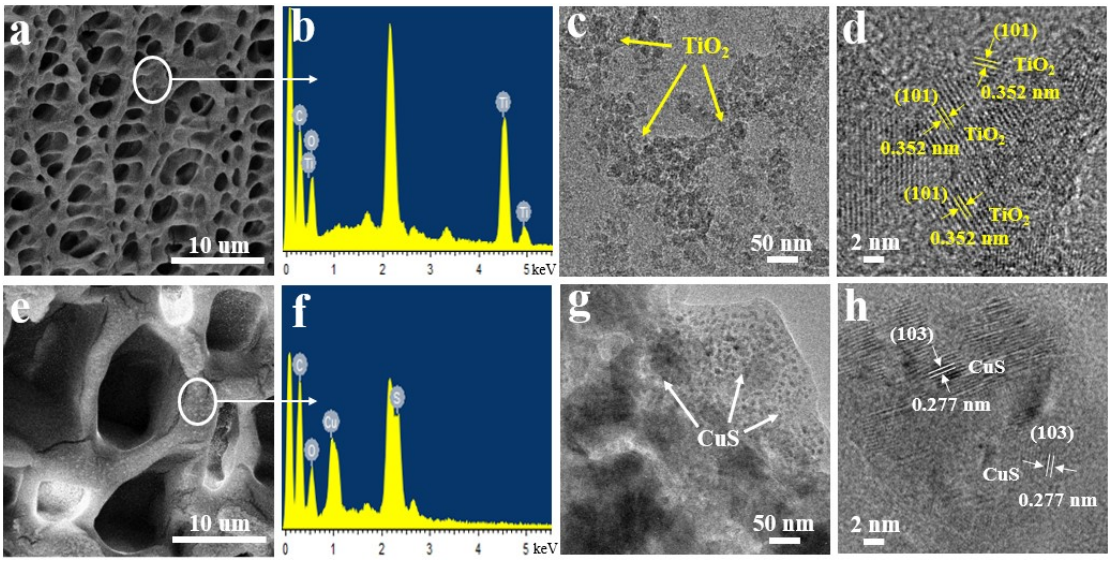

Fig. S1. SEM image (a), EDS (c), TEM image (c) and HRTEM image (d) of PDMAA-TiO_2 hydrogel; SEM image (e), EDS (f), TEM image (g) and HRTEM image (h) of PDMAA-CuS hydrogel.

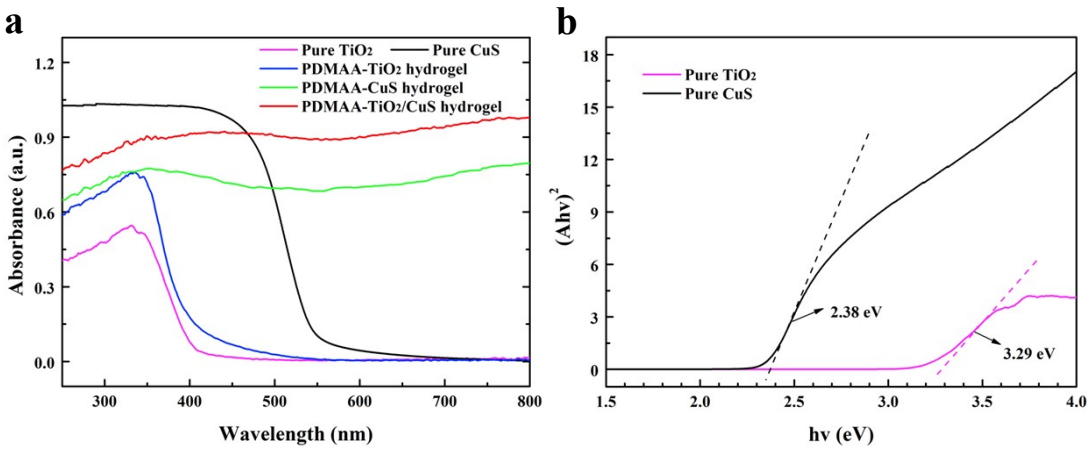

Fig. S2. a) UV-vis diffuse reflectance spectra of TiO_2 particles, CuS particles, PDMAA-TiO_2, PDMAA-CuS and PDMAA-TiO_2/CuS hydrogel. b) The band gap evaluation for linear dependence of $(Ahv)^2$ versus hv for TiO_2 and CuS.

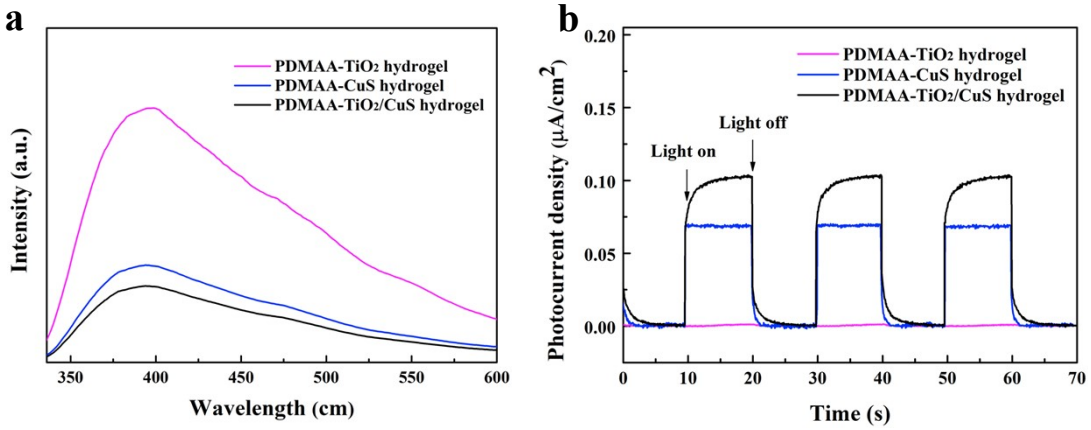

Fig. S3. a) Photoluminescence spectra of PDMAA-TiO_2, PDMAA-CuS and PDMAA-TiO_2/CuS hydrogel. b) The transient photocurrent response of PDMAA-TiO_2, PDMAA-CuS and PDMAA-TiO_2/CuS photocatalyst electrodes with light on-off cycles under visible light irradiation.

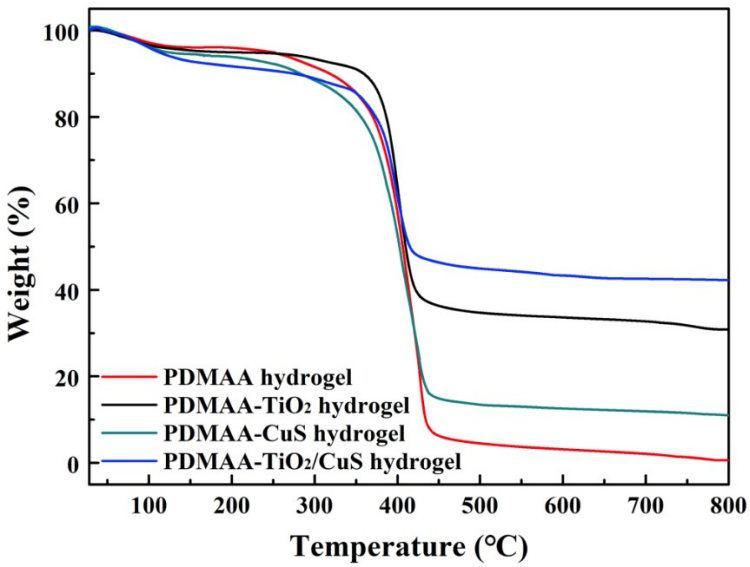

Fig. S4. TGA curves of PDMAA, PDMAA-TiO_2, PDMAA-CuS, and PDMAA-TiO_2/CuS hydrogels.

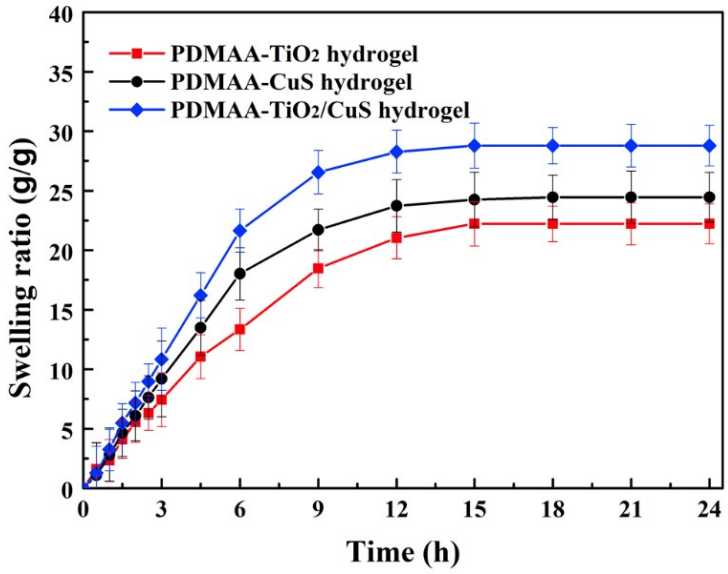

Fig. S5. The swelling ratio of PDMAA-TiO_2, PDMAA-CuS and PDMAA-TiO_2/CuS hydrogel.

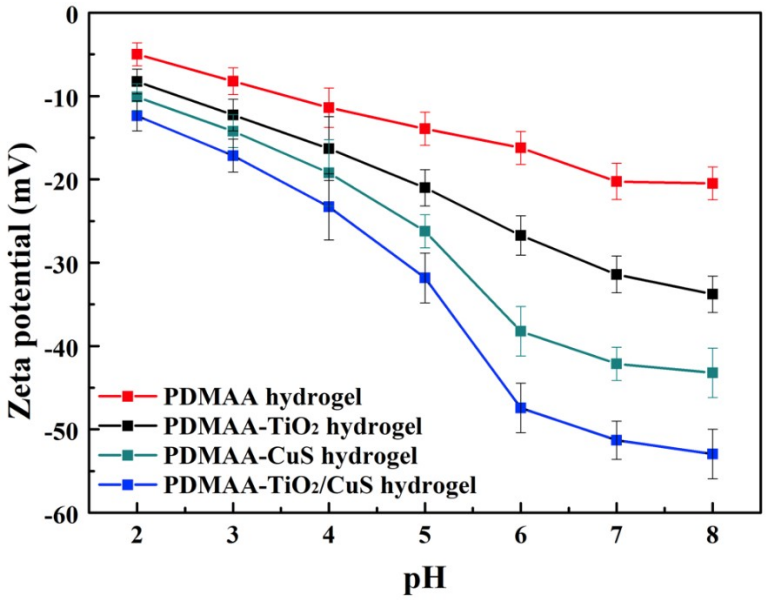

Fig. S6. Zeta potentials of PDMAA, PDMAA-TiO_2, PDMAA-CuS and PDMAA-TiO_2/CuS hydrogel.

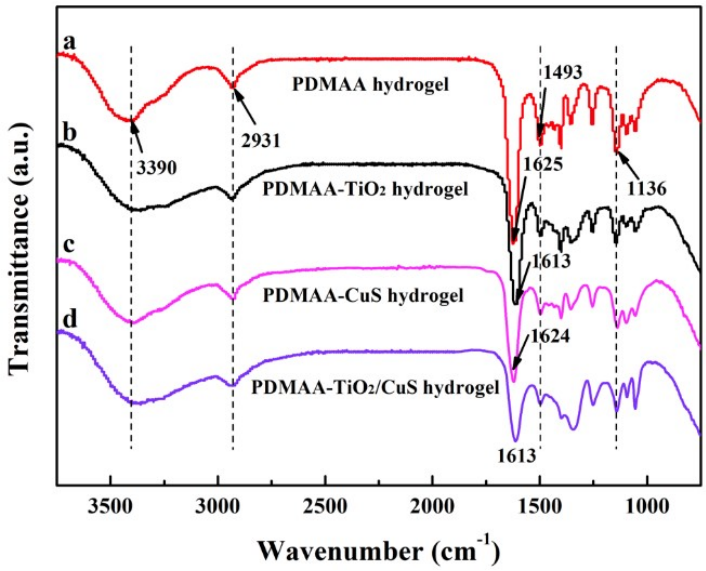

Fig. S7. FTIR spectra (a) PDMAA, (b) PDMAA-TiO_2, (c) PDMAA-CuS, and (d) PDMAA-TiO_2/CuS hydrogel.

The FT-IR spectrum of PDMAA, PDMAA-TiO_2, PDMAA-CuS, and PDMAA-TiO_2/CuS were displayed in Fig. S7. A broad peak around 3390 cm^{-1} was attributed to O-H stretching vibration. The peak at 2931 cm^{-1} was the result of the C-H stretching vibration. The absorption peaks at 1493 cm^{-1} and 1136 cm^{-1} were assigned to C-N stretching and bending vibrations, respectively. The stretch vibration peak of the carbonyl groups of PDMAA shifted from 1625 cm^{-1} to lower wavenumber field at 1613 cm^{-1} in the FTIR spectra, which was the evidence of hydrogen bonding interaction between the polymer chains and TiO_2 nanoparticles during curing process [1]. After loaded CuS, the FTIR spectra peak at 1613 cm^{-1} weakened dramatically compared with PDMAA-TiO_2, which could be explained by the fact that carbonyl groups were the major function groups that interacted with CuS [2].

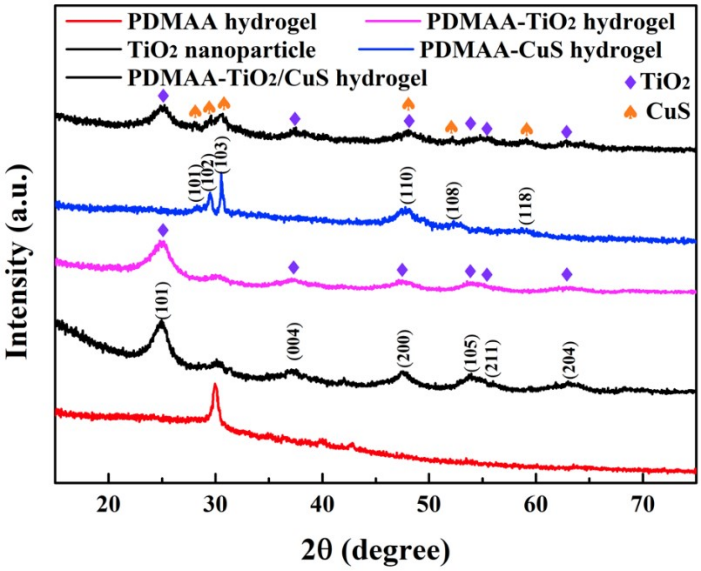

Fig. S8. XRD spectra of TiO_2 nanoparticle, and PDMAA, PDMAA-TiO_2, PDMAA-CuS and PDMAA-TiO_2/CuS hydrogel.

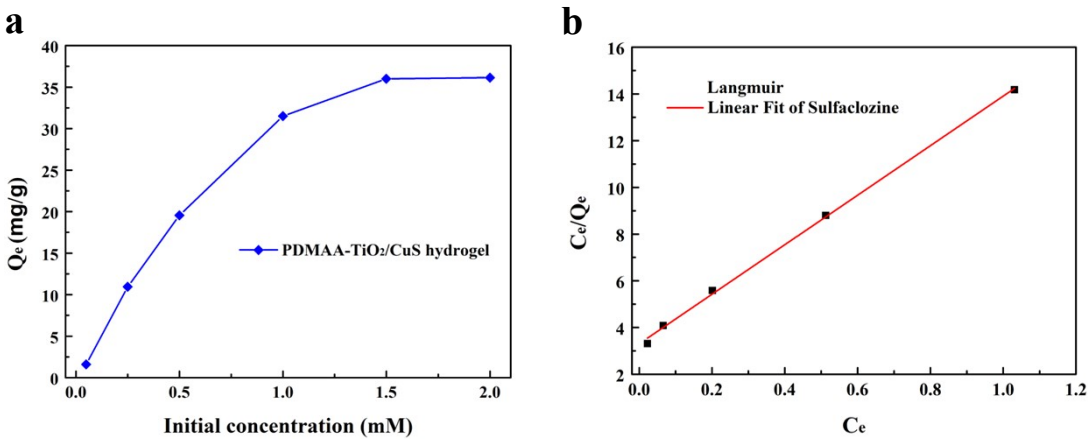

Fig. S9. a) Adsorption isotherm analyses of sulfaclozine on PDMAA-TiO_2/CuS hydrogel. b) Adsorption isotherm analyses with Langmuir model of sulfaclozine on PDMAA-TiO_2/CuS hydrogel.

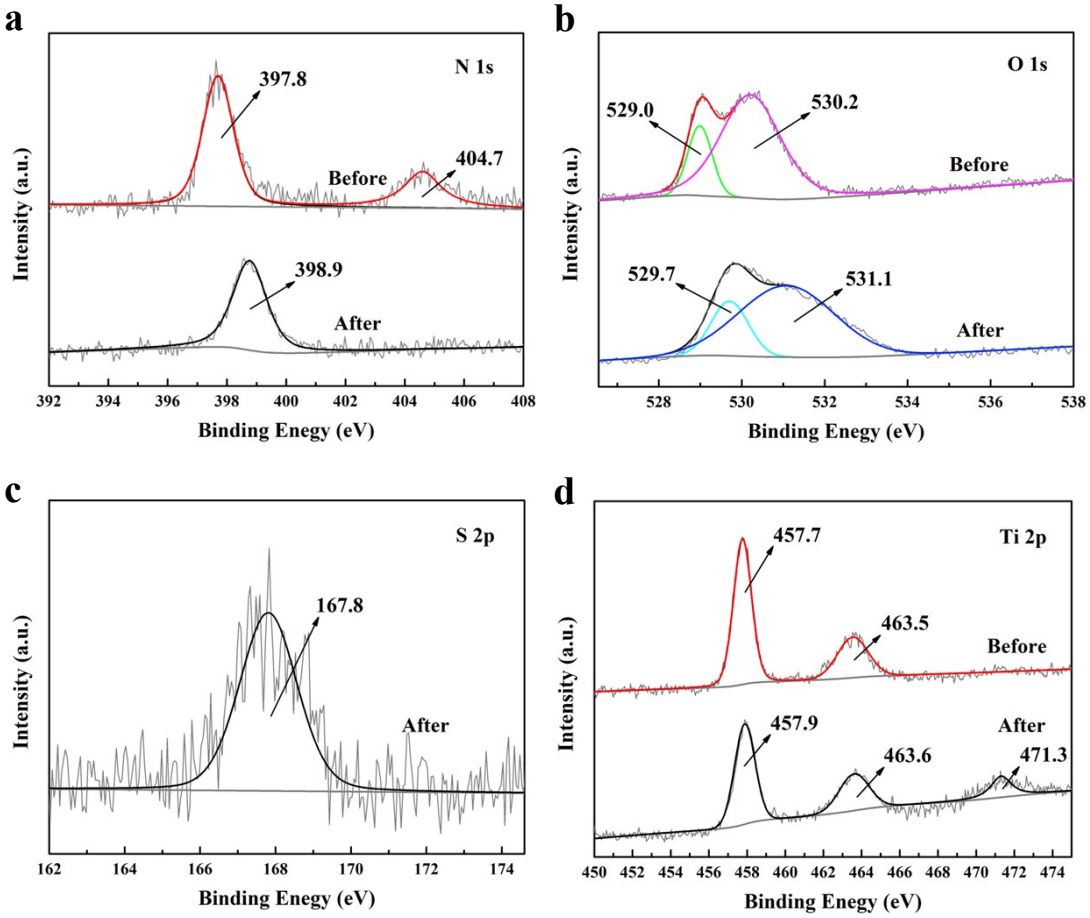

Fig. S10. High-resolution XPS spectra (a) N 1s, (b) O 1s, (c) S 2p, (d) Ti 2p of PDMAA-TiO_2 hydrogel before and after the adsorption of sulfaclozine.

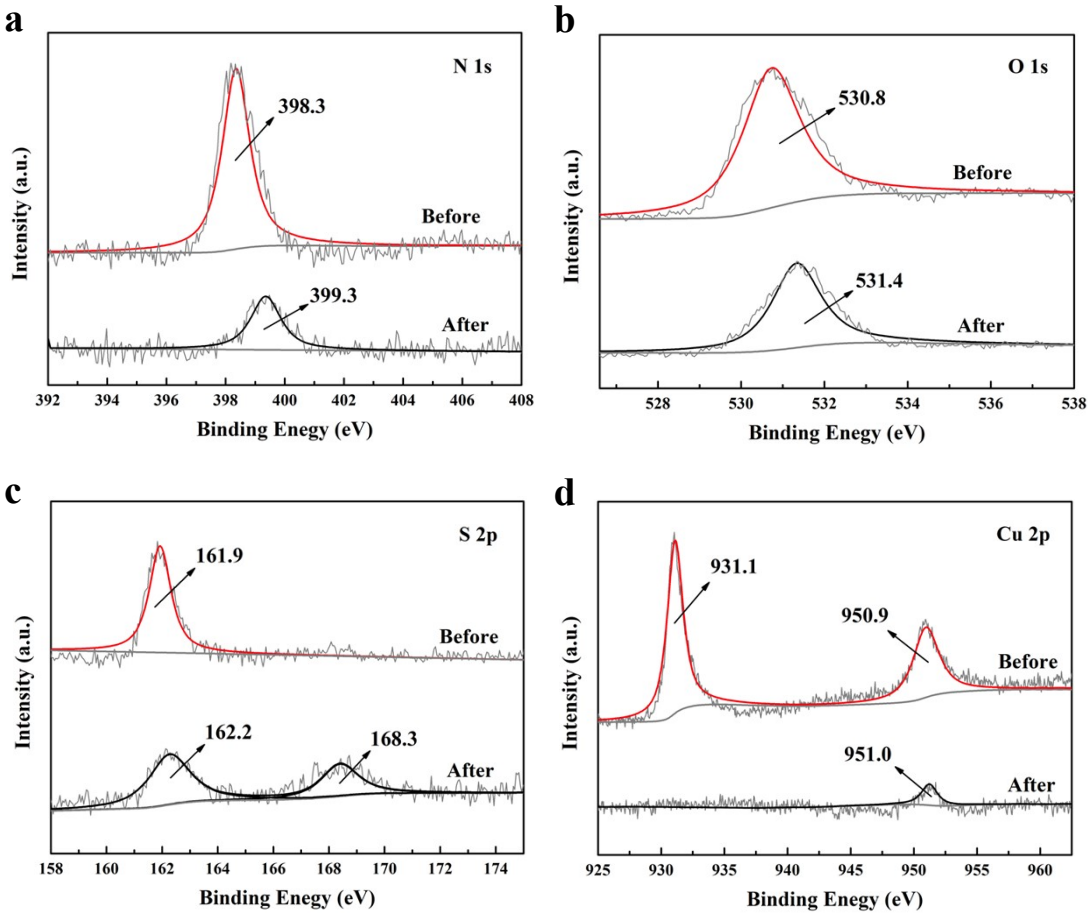

Fig. S11. High-resolution XPS spectra (a) N 1s, (b) O 1s, (c) S 2p, (d) Cu 2p of PDMAA-CuS hydrogel before and after the adsorption of sulfaclozine.

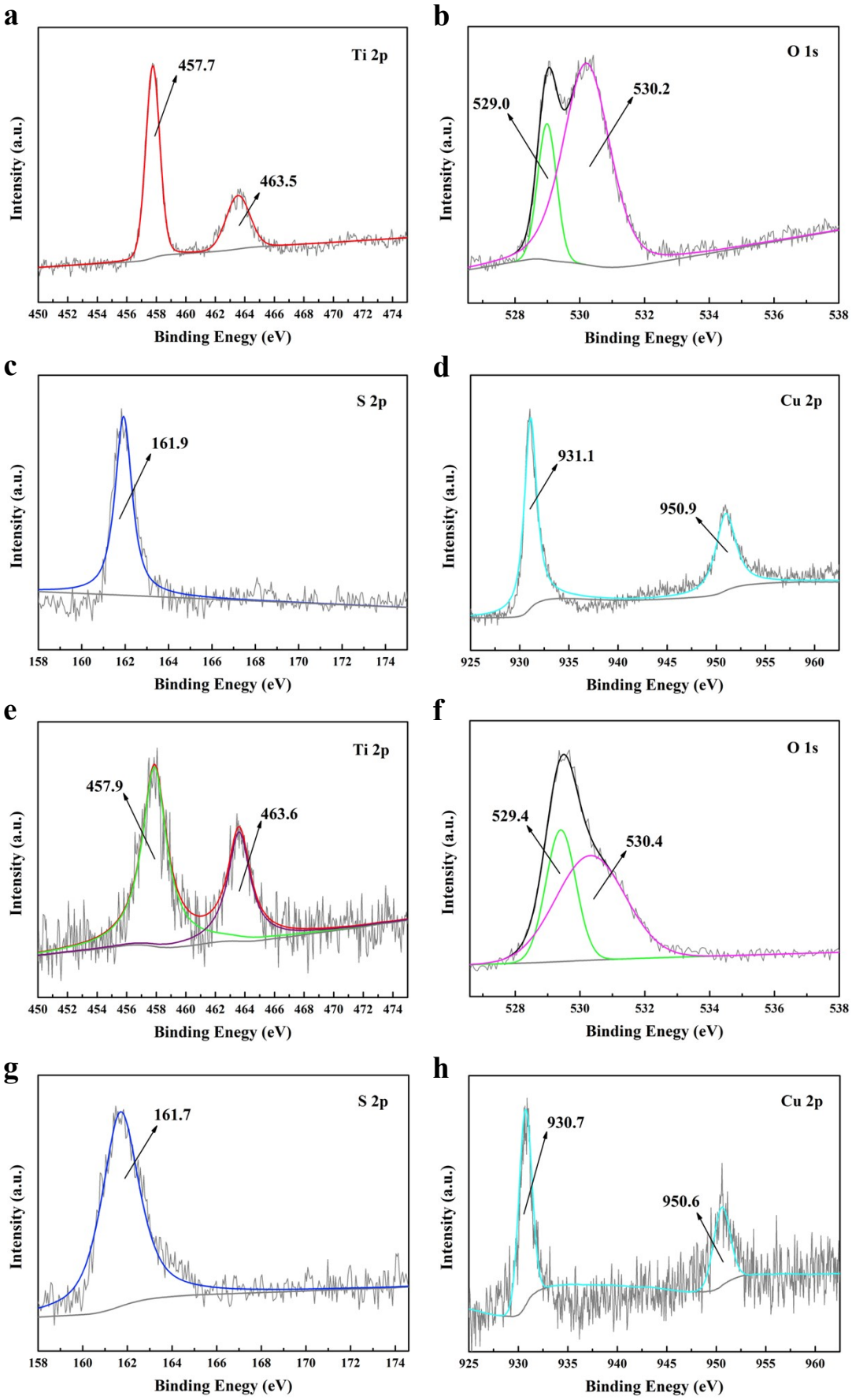

Fig. S12. High-resolution XPS spectra of (a) Ti 2p and (b) O 1s for PDMAA-TiO_2, (c)

S 2p and (d) Cu 2p for PDMAA-CuS, and (e) Ti 2p, (f) O 1s, (g) S 2p, and (h) Cu 2p for PDMAA-TiO_2/CuS composite.

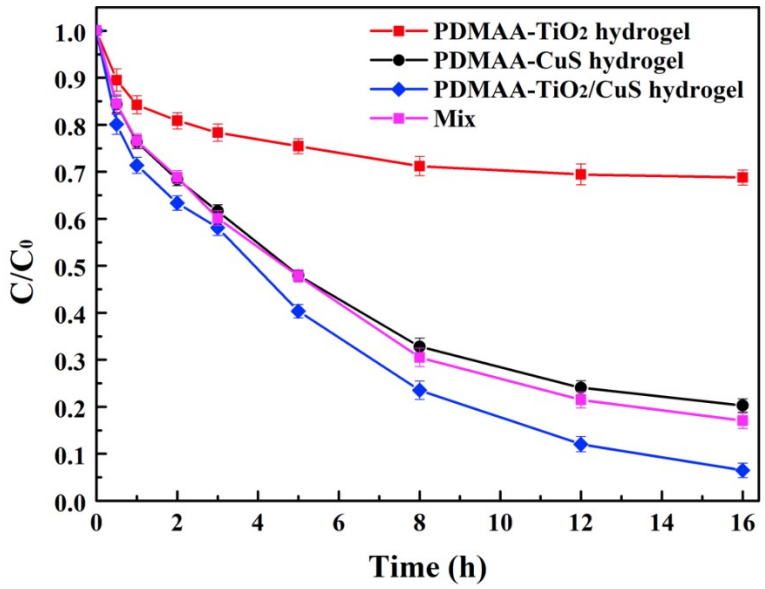

Fig. S13. The photodegradation rate of sulfaclozine using PDMAA-TiO_2, PDMAA-CuS, PDMAA-TiO_2/CuS hydrogel, and mix (PDMAA-CuS hydrogel and TiO_2 nanoparticles) with 300W visible light.

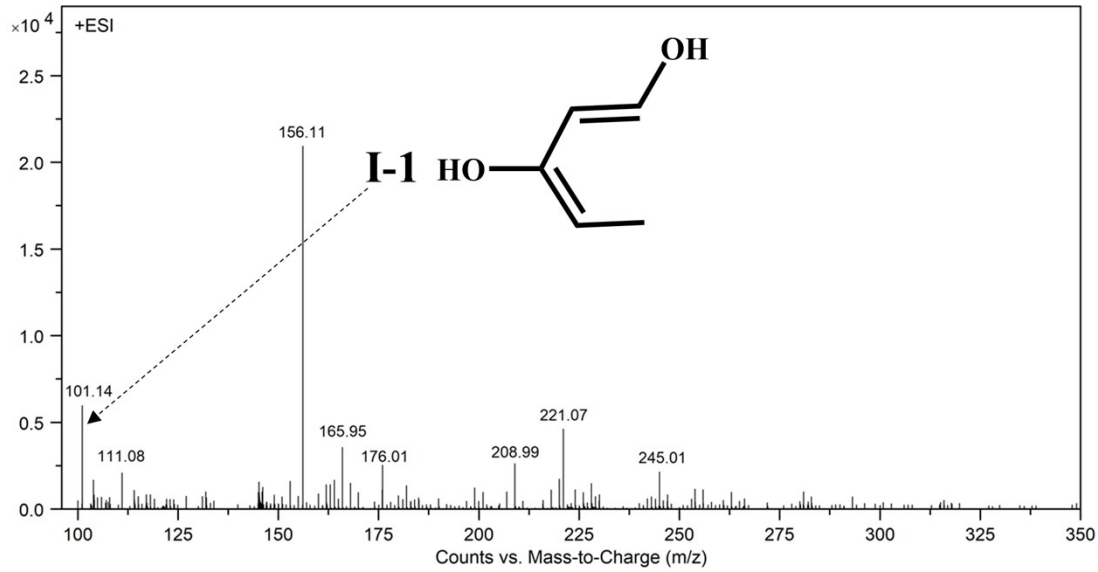
×10 4
+ESI
I-1
HO
OH
156.11
101.14
111.08
165.95
176.01
208.99
221.07
245.01
Counts vs. Mass-to-Charge (m/z)

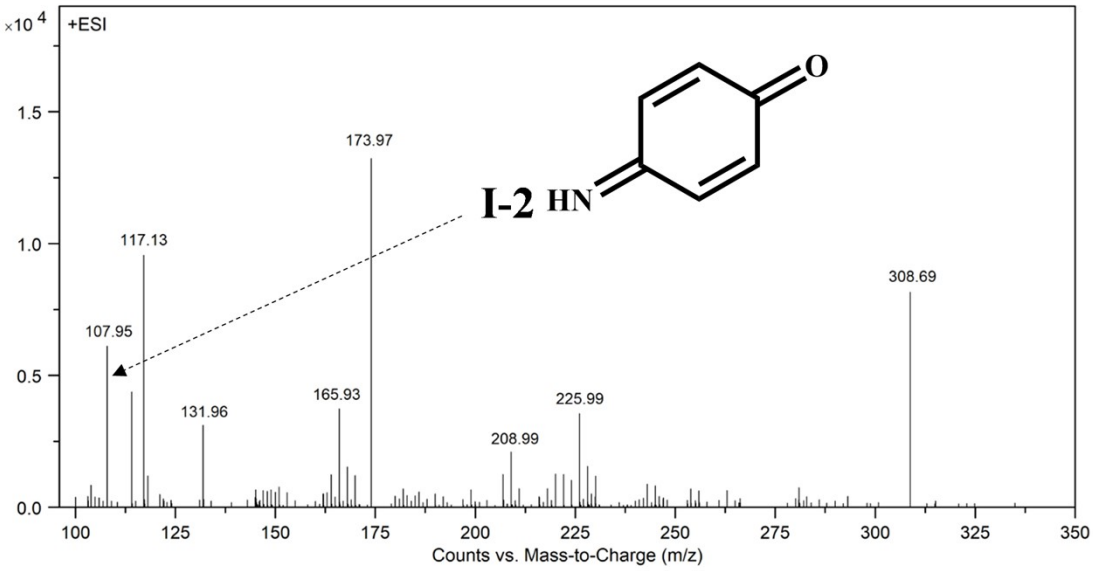
×10 4
+ESI
I-2
HN
O
173.97
117.13
107.95
131.96
165.93
208.99
225.99
308.69
Counts vs. Mass-to-Charge (m/z)

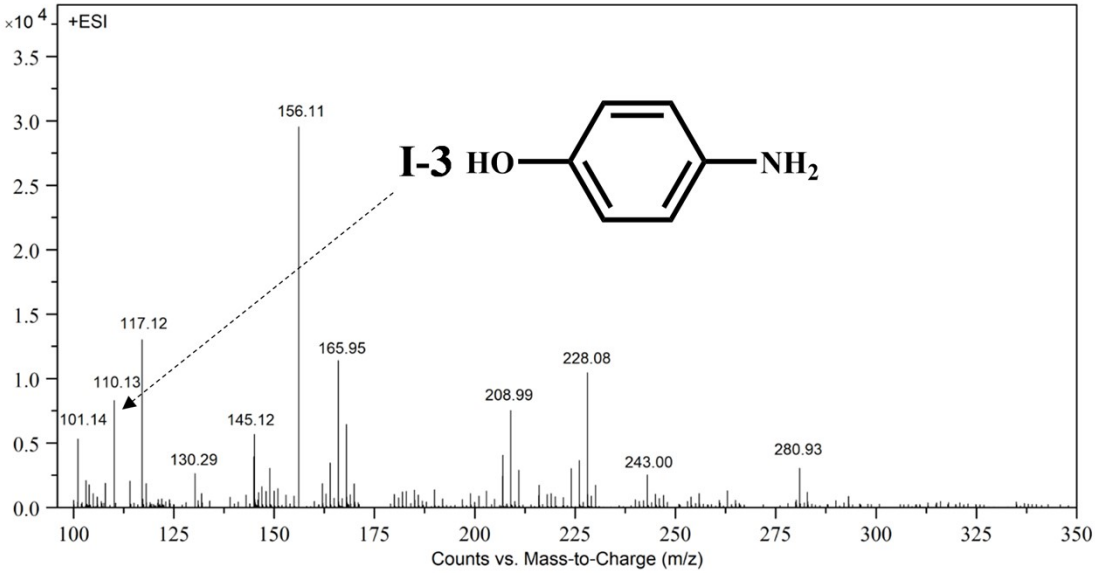
×10 4
+ESI
I-3
HO
NH2
156.11
117.12
110.13
101.14
130.29
145.12
165.95
208.99
228.08
243.00
280.93
Counts vs. Mass-to-Charge (m/z)

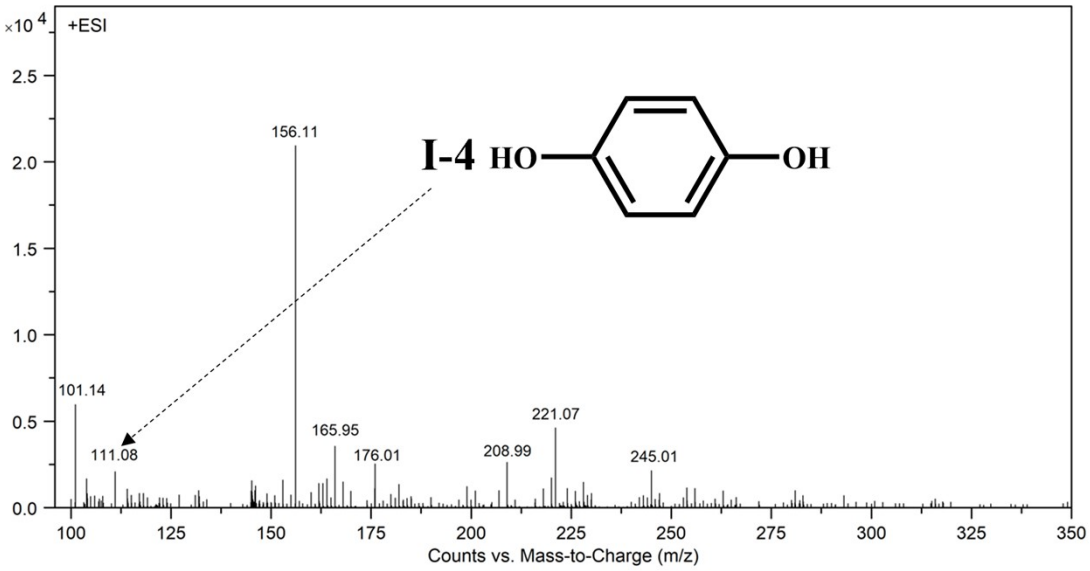
×10 4
+ESI
I-4
HO
OH
156.11
101.14
111.08
165.95
176.01
208.99
221.07
245.01
Counts vs. Mass-to-Charge (m/z)

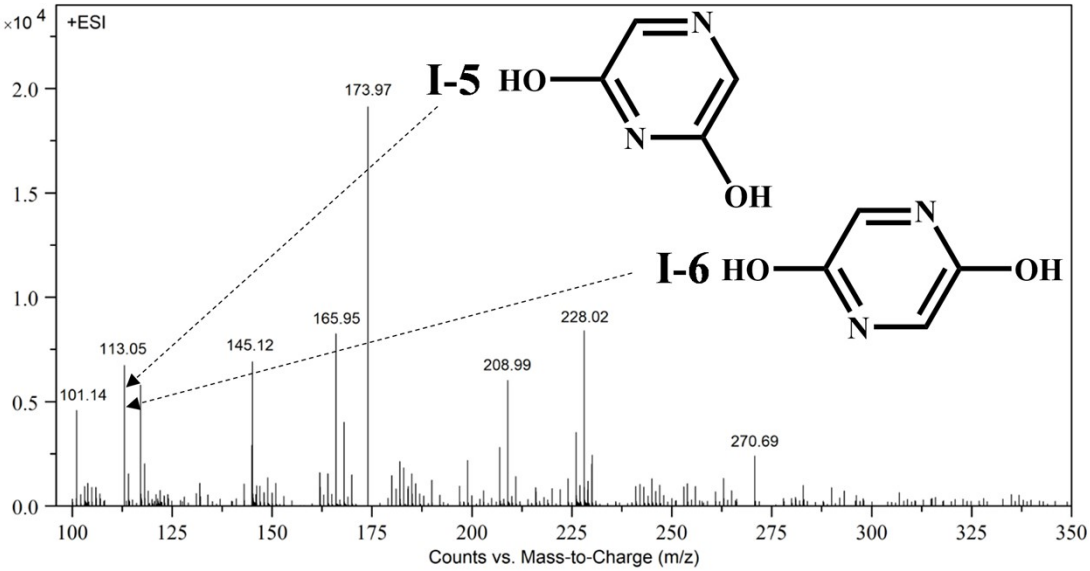
×10 4
+ESI
I-5
HO
N
N
OH
I-6
HO
N
N
OH
173.97
113.05
145.12
165.95
208.99
228.02
101.14
270.69
Counts vs. Mass-to-Charge (m/z)

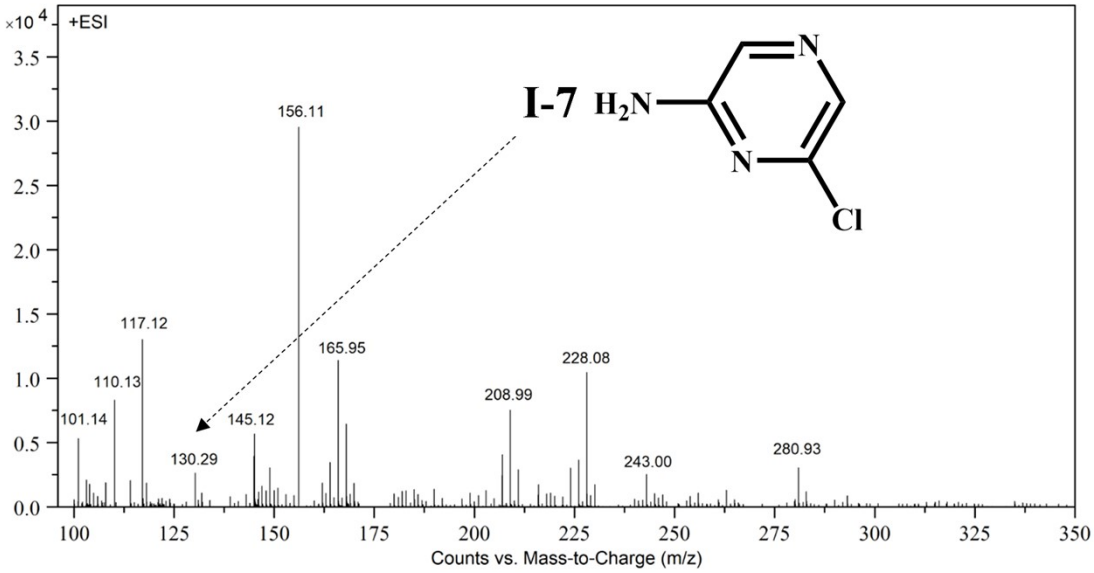
×10 4
+ESI
I-7
H2N
N
N
Cl
156.11
117.12
110.13
101.14
130.29
145.12
165.95
208.99
228.08
243.00
280.93
Counts vs. Mass-to-Charge (m/z)

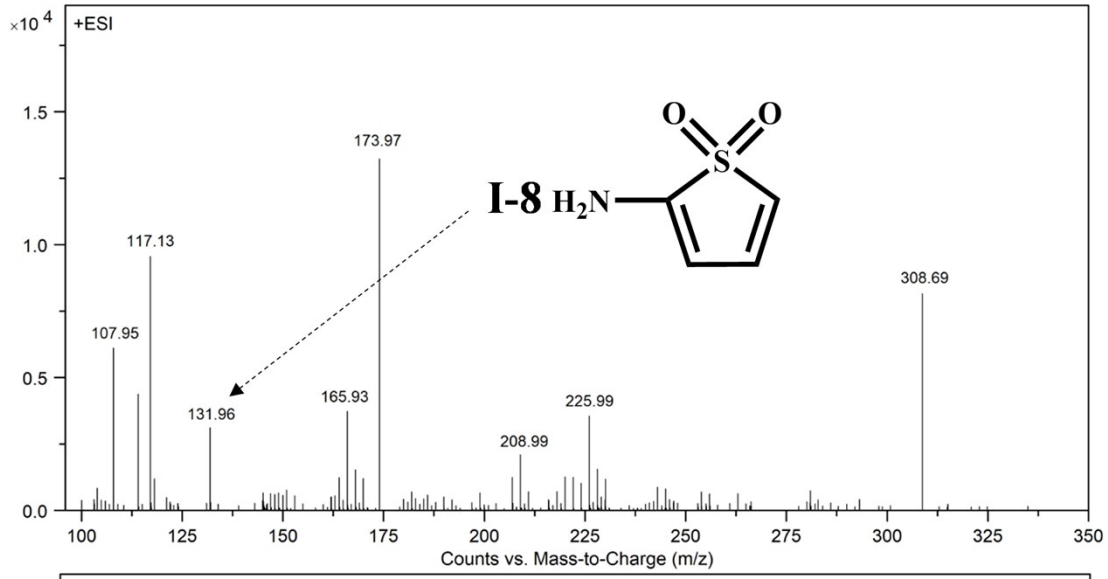
×10 4
+ESI
1.5
1.0
0.5
0.0
173.97
117.13
107.95
131.96
165.93
208.99
225.99
308.69
I-8 H2N
O
O
S
100
125
150
175
200
225
250
275
300
325
350
Counts vs. Mass-to-Charge (m/z)

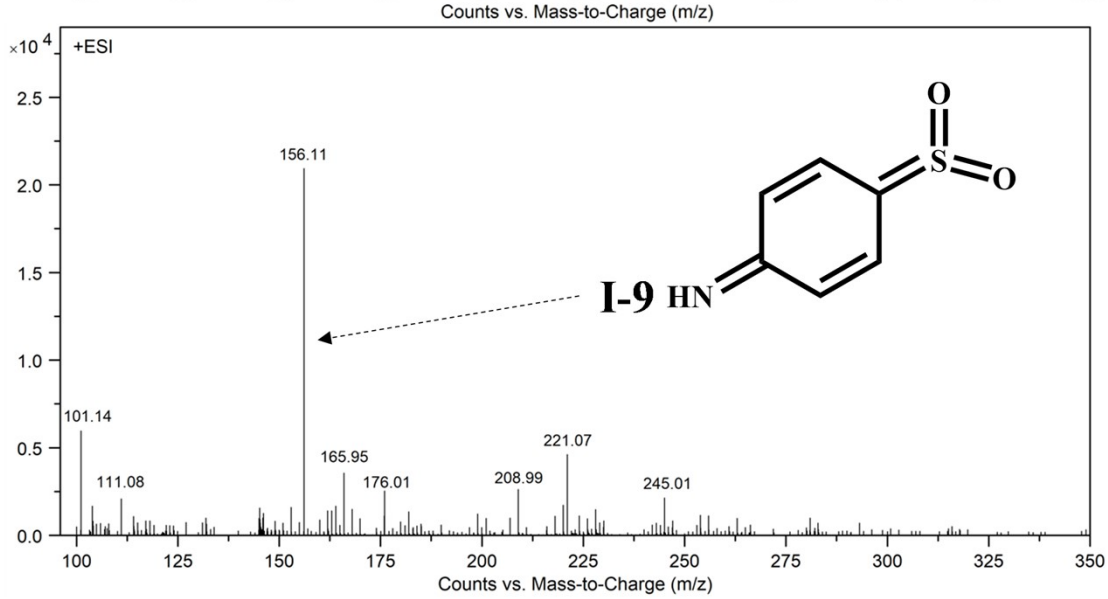
×10 4
+ESI
2.5
2.0
1.5
1.0
0.5
0.0
156.11
101.14
111.08
165.95
176.01
208.99
221.07
245.01
I-9 HN
O
S
O
100
125
150
175
200
225
250
275
300
325
350
Counts vs. Mass-to-Charge (m/z)

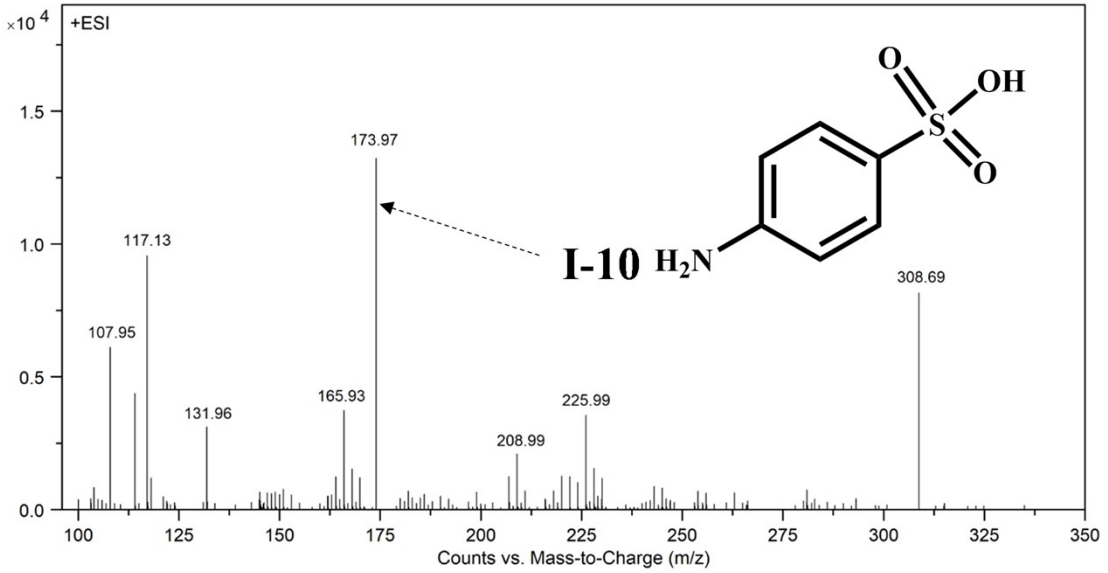
×10 4
+ESI
1.5
1.0
0.5
0.0
173.97
117.13
107.95
131.96
165.93
208.99
225.99
308.69
I-10 H2N
O
OH
S
O
100
125
150
175
200
225
250
275
300
325
350
Counts vs. Mass-to-Charge (m/z)

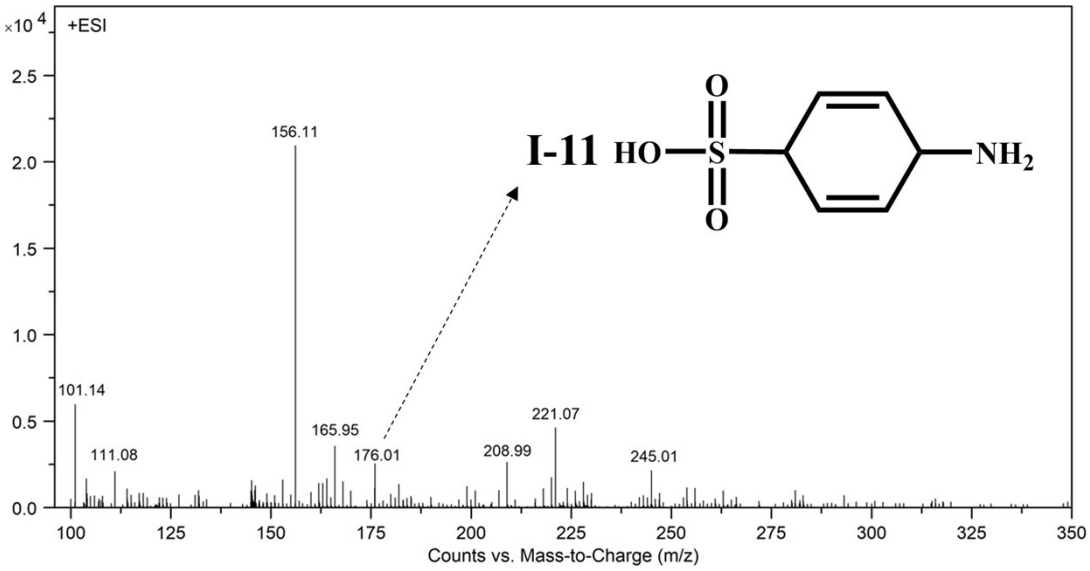
×10 4
+ESI
I-11
HO
S
O
O
NH2
156.11
101.14
111.08
165.95
176.01
208.99
221.07
245.01
Counts vs. Mass-to-Charge (m/z)

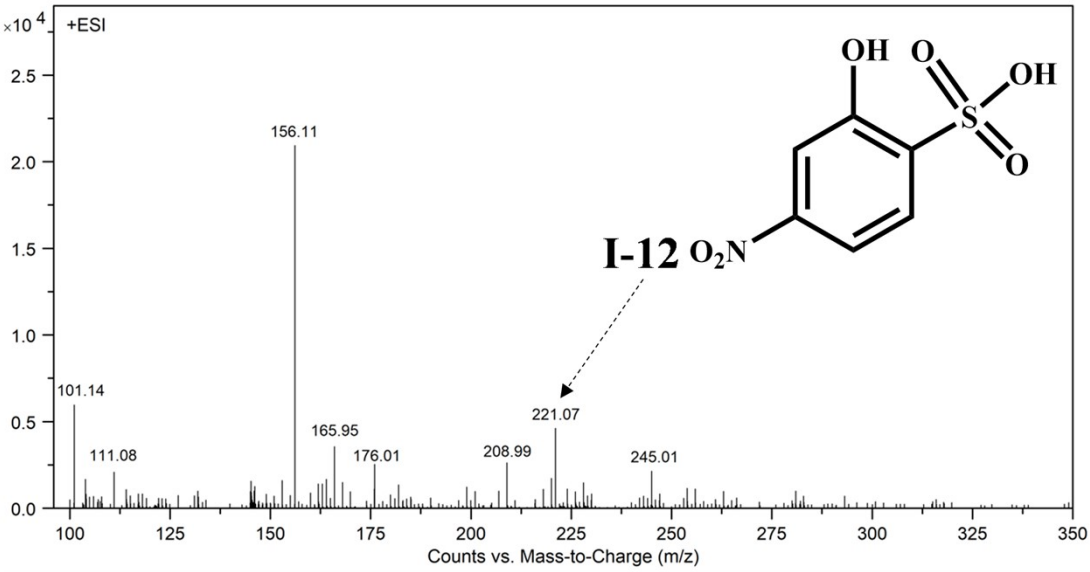
×10 4
+ESI
I-12
OH
O
OH
S
O
O2N
156.11
101.14
111.08
165.95
176.01
208.99
221.07
245.01
Counts vs. Mass-to-Charge (m/z)

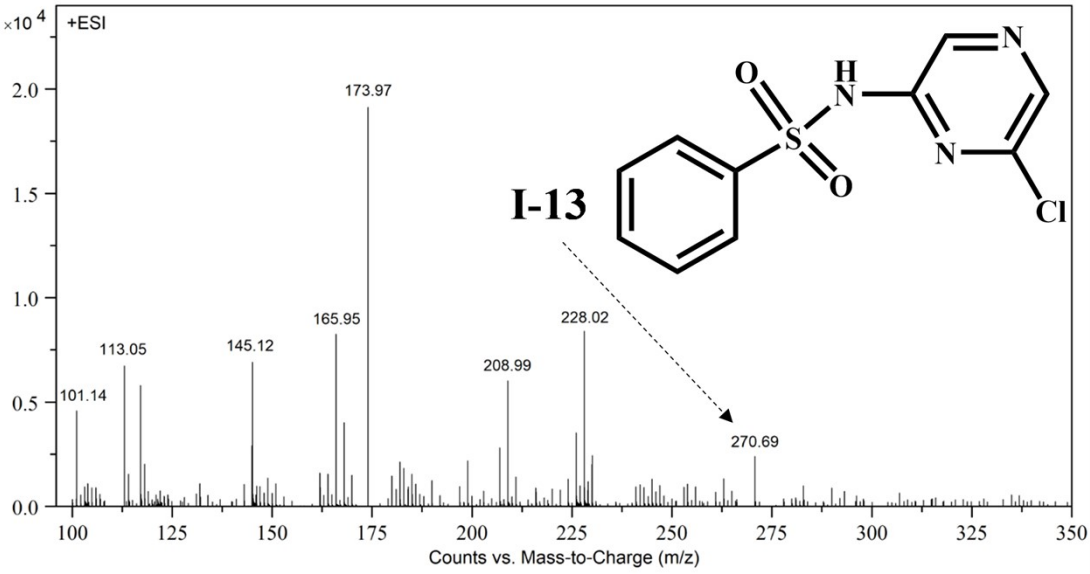
×10 4
+ESI
I-13
O
H
N
S
O
N
N
Cl
173.97
113.05
145.12
165.95
208.99
228.02
101.14
270.69
Counts vs. Mass-to-Charge (m/z)

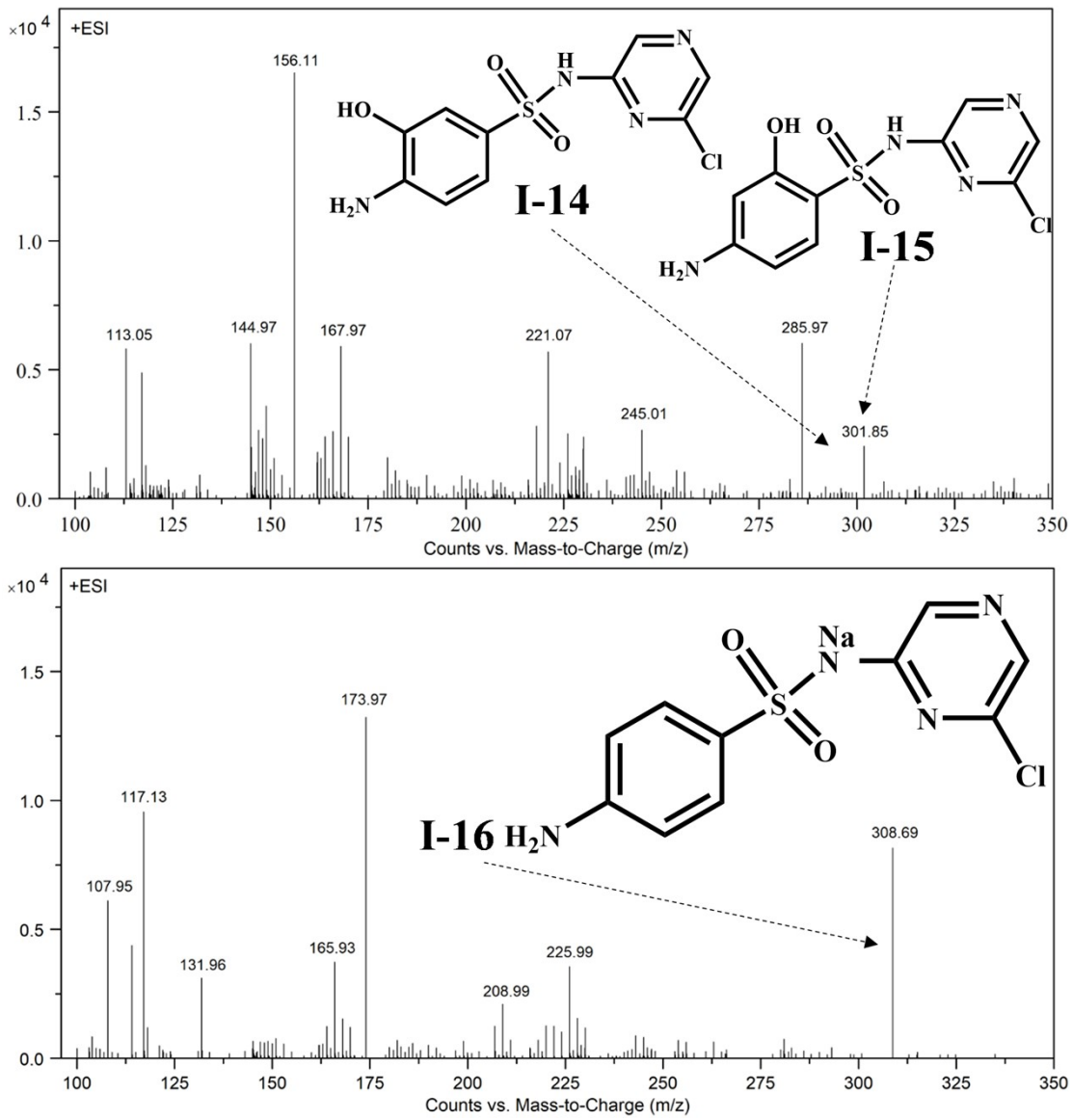

Fig. 14. The MS data and proposed structures of the intermediates of sulfaclozine photodegradation in the composite hydrogel catalysis system.

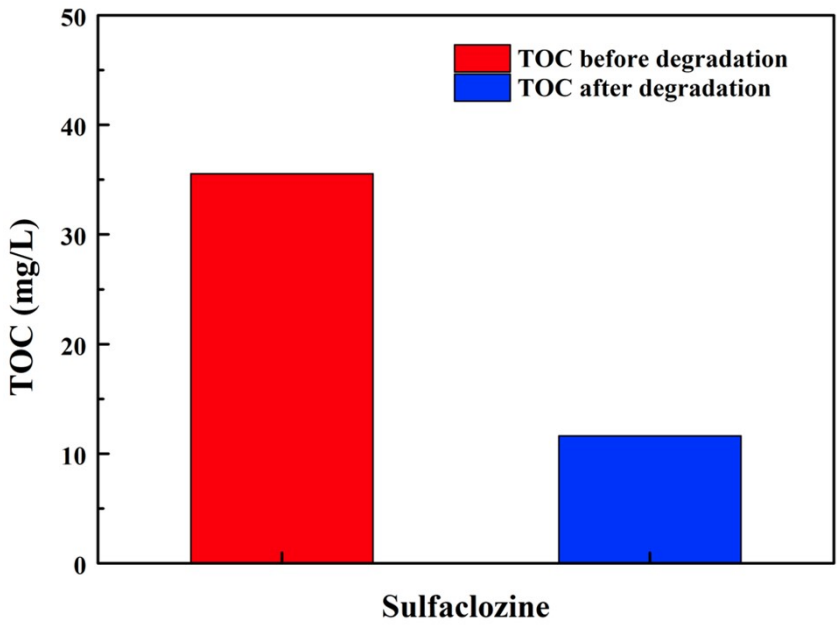

Fig. S15. The TOC removal ratio of sulfaclozine in the composite hydrogel catalysis system.

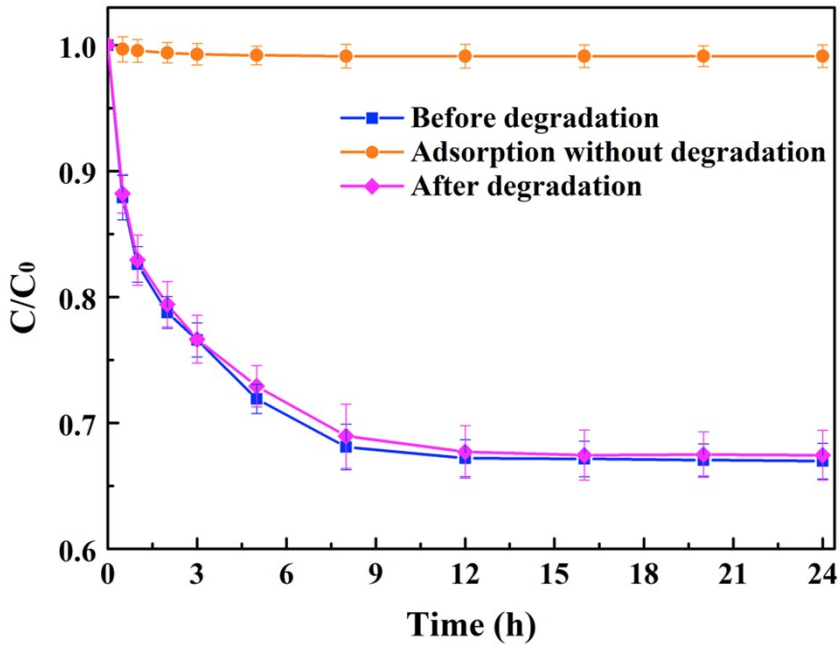

Fig. S16. The curves of the removal rate for sulfaclozine using PDMAA-TiO_2/CuS hydrogels at various circumstances including adsorption before degradation, adsorption again after degradation, and repeating adsorption without degradation.

Table S1. The photodegradation intermediates of sulfaclozine

Product ID	Possible intermediates and structure	$[M+H]^+$	Reported by
I-1	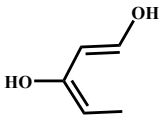	101.14	[3]
I-2	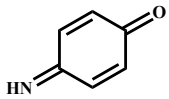	107.95	[4]
I-3		110.13	[2]
I-4		111.08	[5]
I-5	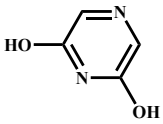	113.05	[5]
I-6	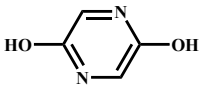	113.05	[5]
I-7	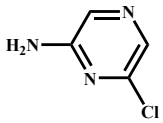	130.29	[6]
I-8	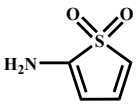	131.96	[5]
I-9	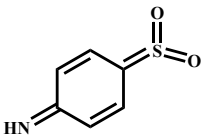	156.11	[7]

Product ID	Possible intermediates and structure	$[M+H]^+$	Reported by
I-10	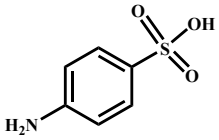	173.97	[8]
I-11	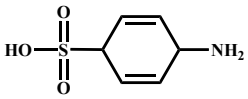	176.01	[9]
I-12	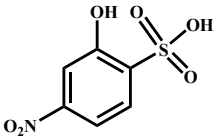	221.07	[3]
I-13	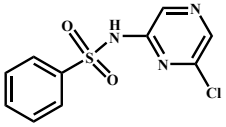	270.69	[2]
I-14	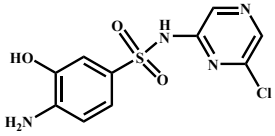	301.85	[10]
I-15	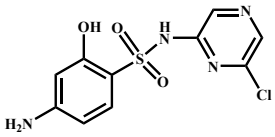	301.85	[11]
I-16	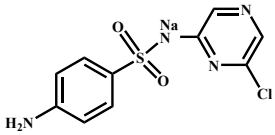	308.69	[12]

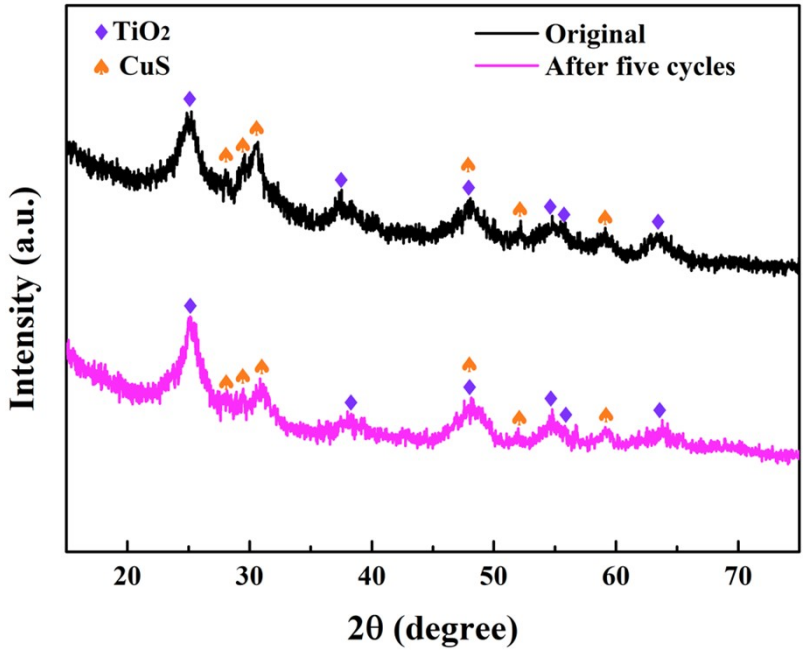

Fig. S17. XRD spectra of PDMAA-TiO_2/CuS hydrogel before and after the cycling test.

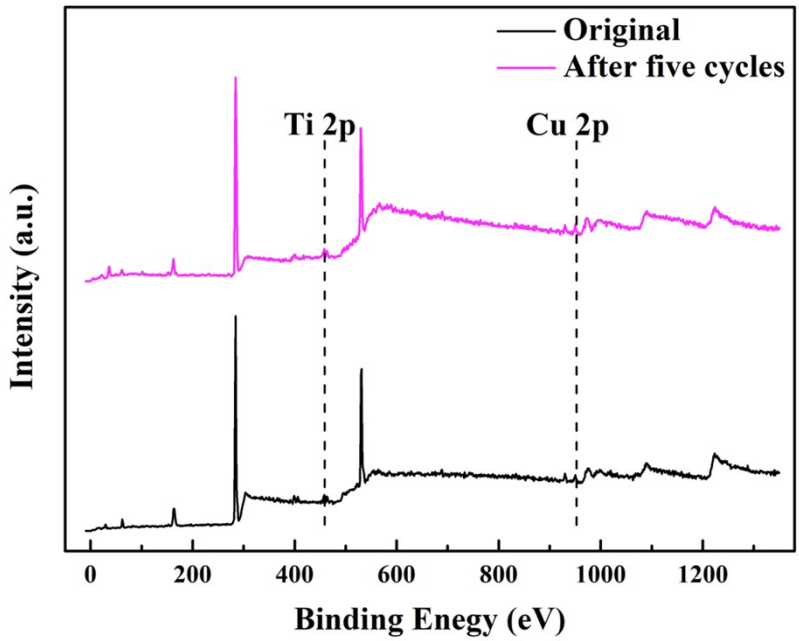

Fig. S18. XPS spectra of PDMAA-TiO_2/CuS hydrogel before and after the cycling test.

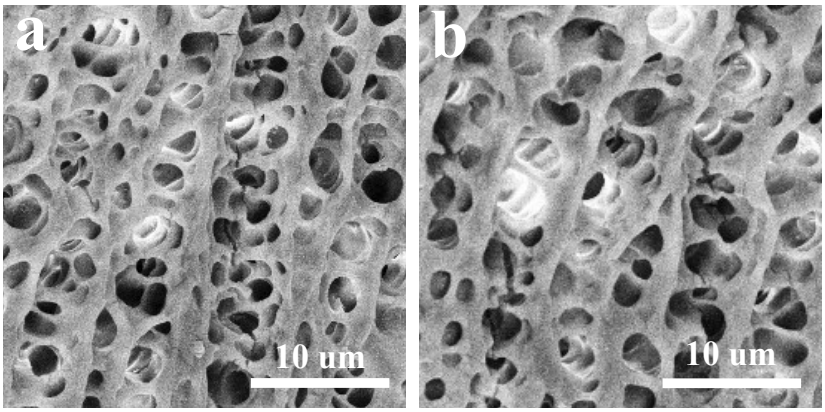

Fig. S19. The SEM images of PDMAA-TiO_2/CuS hydrogel (a) before and (b) after the cycling test.

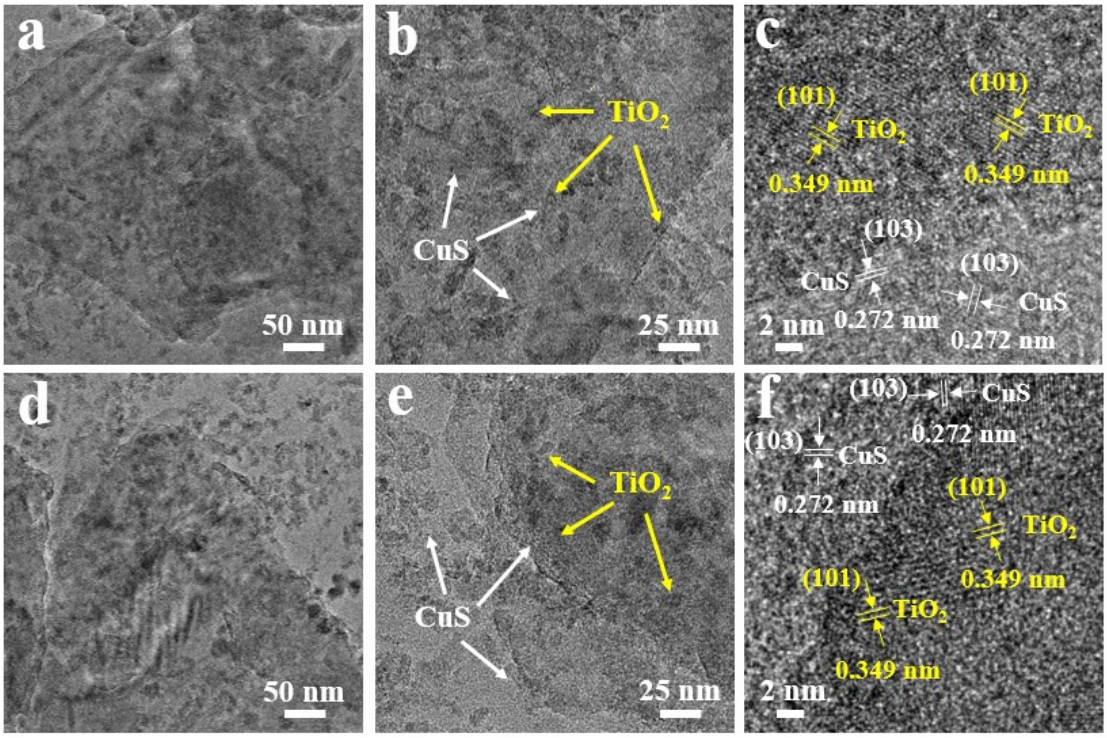

Fig. S20. The TEM images of PDMAA-TiO_2/CuS hydrogel (a,b,c) before and (d, e, f) after the cycling test.

Table S2. Property comparison of photocatalysts reported in recent three years for degradation of antibiotics under visible light irradiation.

	Photocatalyst	Target contaminant	Separation free	Adsorption	Optimum photodegradation	Mineralization	Reusability	Year	Ref.
1	MoS_2 /graphene aerogel	Tetracycline	Yes	-	10.00%	-	Yes	2019	[13]
2	Bi_2O_3/Bi_2MoO_6	Tetracycline	N/A	-	70.00%	-	Yes	2019	[14]
3	$In_2S_3/InVO_4$	Tetracycline	N/A	-	71.41%	61.14%	Yes	2019	[15]
4	W-doped $BaTiO_3$	Tetracycline	N/A	15.00%	80.00%	-	Yes	2019	[16]
5	TCPP/rGO/Bi_2WO_6	Tetracycline	N/A	-	84.00%	-	Yes	2019	[17]
6	Ce^{3+} doped Bi_2O_3	Tetracycline	N/A	-	89.10%	-	N/A	2019	[18]
7	Ti^{3+}/N co-doped TiO_2/DG	Tetracycline	N/A	-	92.00%	-	N/A	2019	[19]
8	BiOCl/TiO_2 composite	Tetracycline	N/A	28.27%	84.04%	-	Yes	2020	[20]
9	MoS_2/g-C_3N_4/$Bi_{24}O_{31}Cl_{10}$	Tetracycline	N/A	-	97.50%	-	Yes	2020	[21]
10	Z-scheme Bi_2WO_6-P25	Tetracycline	N/A	-	89.00%	51.00%	Yes	2021	[22]
11	CoP/ZnSnO3	Tetracycline	N/A	-	96.44%	-	N/A	2021	[23]
12	Pt/$BiVO_4$ Nanosheets	Tetracycline	N/A	-	88.50%	-	N/A	2021	[24]
13	Cu_2O nanostructures	Trimethoprim	N/A	-	77.29%	-	N/A	2021	[25]
14	Bi (Spheres)/g-C_3N_4	Amoxicillin	N/A	-	5.00%	-	N/A	2019	[26]

Photocatalyst	Target contaminant	Separation free	Adsorption	Optimum photodegradation	Mineralization	Reusability	Year	Ref.
15 Pt-Bi co-doped TiO_2	Amoxicillin	N/A	-	87.67%	-	N/A	2019	[27]
16 Mesoporous g-C_3N_4	Amoxicillin	N/A	-	90.00%	25.00%	Yes	2020	[28]
17 Cu doped TiO_2	Amoxicillin	N/A	-	90.00%	-	N/A	2020	[29]
18 CuI/$FePO_4$	Amoxicillin	N/A	-	90.00%	-	Yes	2022	[30]
19 TiO_2/Bi_2MoO_6	Amoxicillin	N/A	-	94.10%	65.40%	Yes	2022	[31]
20 Fe_3O4@SiO_2@MIL-53-NH_2	Ampicillin	N/A	-	70.00%	-	Yes	2020	[32]
21 C_3N_4-MoS_2/3DG	Ampicillin	N/A	-	74.60%	26.87%	N/A	2021	[33]
22 Bi/Bi_3NbO_7 nanosheets	Ciprofloxacin	N/A	-	86.00%	53.00%	N/A	2019	[34]
23 Polyaniline/$Bi_4O_5Br_2$	Ciprofloxacin	N/A	23.03%	99.00%	-	Yes	2019	[35]
24 Fe_3O_4/CdS/g-C_3N_4	Ciprofloxacin	N/A	-	81.00%	-	N/A	2020	[36]
25 N-doped TiO_2 nanoparticles	Ciprofloxacin	N/A	-	54.50%	26.00%	N/A	2020	[37]
26 Ag-TiO_2	Ciprofloxacin	N/A	-	92.00%	-	Yes	2021	[38]
27 Bi_2O_3-modified La-$NaTaO_3$	Ciprofloxacin	N/A	-	83.00%	-	Yes	2021	[39]
28 g-C_3N_4/Zn doped Fe_3O_4	Cephalexin	N/A	-	91.00%	80.50%	Yes	2019	[40]
29 Urea/TiO_2/$ZnFe_2O_4$/zeolite	Cephalexin	N/A	-	95.00%	-	Yes	2020	[41]

Photocatalyst	Target contaminant	Separation free	Adsorption	Optimum photodegradation	Mineralization	Reusability	Year	Ref.
30 $CuWO_4/Bi_2S_3/ZIF67$	Cephalexin	N/A	-	90.10%	74.00%	Yes	2020	[42]
31 z-scheme $MoO_3/Ag/C_3N_4$	Ofloxacin	N/A	33.00%	96.00%	60.00%	Yes	2020	[43]
32 N-TiO_2 coupled $BiVO_4$	Ofloxacin	N/A	-	92.00%	78.00%	Yes	2021	[44]
33 $LaFeO_3$/lignin-biochar	Ofloxacin	N/A	26.71%	95.60%	-	Yes	2022	[45]
34 Biochar-based Zn-TiO_2/pBC	Sulfamethoxazole	N/A	-	81.21%	56.13%	Yes	2019	[46]
35 Fe_3O_4 modified BiOCl/$BiVO_4$	Sulfamethoxazole	N/A	-	91.00%	-	N/A	2019	[47]
36 MnO_2 incorporating Fe_2O_3	Sulfamethoxazole	N/A	-	90.00%	-	Yes	2020	[3]
37 α-Fe_2O_3@graphene	Sulfamethoxazole	N/A	-	92.00%	-	N/A	2020	[48]
38 Silicate glass@$Cu_2O/Cu_2V_2O_7$	Sulfamethoxazole	N/A	-	90.10%	83.20%	Yes	2021	[49]
39 Ag_2O-$KNbO_3$	Sulfamethoxazole	N/A	-	92.00%	-	N/A	2021	[50]
40 PDMAA-TiO_2/CuS hydrogel	Sulfaclozine	Yes	32.96%	97.86%	67.53%	Yes	This work	

References

[1] R. Tamaki, K. Naka, T. Chujo, Synthesis of poly(N,N'-dimethylacrythlamide)/silica gel polymer hybrids by in situ polymerization method, Ploym. J., 30 (1998) 60-65.

[2] J. H. Yang, Z. K. Li, H. J. Zhu, Adsorption and photocatalytic degradation of sulfamethoxazole by a novel composite hydrogel with visible light irradiation, Appl. Catal. B, 217 (2017) 603-614.

[3] R. Guo, Y. Wang, J. Li, X. Cheng, D.D. Dionysiou, Sulfamethoxazole degradation by visible light assisted peroxymonosulfate process based on nanohybrid manganese dioxide incorporating ferric oxide, Appl. Catal. B, 278 (2020) 119297.

[4] M. Jahdi, S.B. Mishra, E.N. Nxumalo, S.D. Mhlanga, A.K. Mishra, Smart pathways for the photocatalytic degradation of sulfamethoxazole drug using F-Pd co-doped TiO2 nanocomposites, Appl. Catal. B, 267 (2020) 118716.

[5] L. Ismail, A. Rifai, C. Ferronato, L. Fine, F. Jaber, J. Chovelon, Towards a better understanding of the reactive species involved in the photocatalytic degradation of sulfaclozine, Appl. Catal. B, 185 (2016) 88-99.

[6] P. Calza, Photocatalytic transformations of sulphonamides on titanium dioxide, Appl. Catal. B, 53 (2004) 63-69.

[7] G. Liu, X. Li, B. Han, L. Chen, L. Zhu, L.C. Campos, Efficient degradation of sulfamethoxazole by the Fe(II)/HSO^{5-}process enhanced by hydroxylamine: Efficiency and mechanism, J. Hazard. Mater., 322 (2017) 461-468.

[8] A. Fabianska, A. Bialk-Bielinska, P. Stepnowski, S. Stolte, E.M. Siedlecka, Electrochemical degradation of sulfonamides at BDD electrode: kinetics, reaction pathway and eco-toxicity evaluation, J. Hazard. Mater., 280 (2014) 579-587.

[9] H. Gong, W. Chu, Determination and toxicity evaluation of the generated products in sulfamethoxazole degradation by UV/CoFe2O4/TiO2, J. Hazard. Mater., 314 (2016) 197-203.

[10] K. Li, P. Zhang, L. Ge, H. Ren, C. Yu, X. Chen, Y. Zhao, Concentration-dependent photodegradation kinetics and hydroxyl-radical oxidation of phenicol antibiotics, Chemosphere, 111 (2014) 278-282.

[11] A. Dirany, I. Sires, N. Oturan, A. Ozcan, M.A. Oturan, Electrochemical treatment of the antibiotic sulfachloropyridazine: kinetics, reaction pathways, and toxicity evolution, Environ. Sci. Technol., 46 (2012) 4074-4082.

[12] L. Ismail, C. Ferronato, L. Fine, F. Jaber, J. Chovelon, Elimination of sulfaclozine from water with SO^{4-} radicals: Evaluation of different persulfate activation methods, Appl. Catal. B, 201 (2017) 573-581.

[13] X. Yang, Z. Chen, J. Fang, Q. Yang, W. Zhao, X. Qian, D. Zhou, C. Liu, M. Chen, Freestanding 3D MoS_2 nanosheets/graphene aerogel heterostructure as a recyclable photocatalyst for efficiently degrading antibiotic residues, Mater. Lett., 252 (2019) 5-7.

[14] H. Zhen, M.A. Khan, M. Xia, W. Lei, F. Wang, Controllable synthesis of flower-root shaped Bi_2O_3/Bi_2MoO_6 heterostructures as an efficient photocatalyst under visible light irradiation, J. Photochem. Photobiol., A, 372 (2019) 78-88.

[15] X. Yuan, L. Jiang, J. Liang, Y. Pan, J. Zhang, H. Wang, L. Leng, Z. Wu, R. Guan, G. Zeng, In-situ synthesis of 3D microsphere-like $In_2S_3/InVO_4$ heterojunction with efficient photocatalytic activity for tetracycline degradation under visible light irradiation, Chem. Eng. J., 356 (2019) 371-381.

[16] P. Demircivi, E.B. Simsek, Visible-light-enhanced photoactivity of perovskite-type W-doped $BaTiO_3$ photocatalyst for photodegradation of tetracycline, J. Alloy. Compd., 774 (2019) 795-802.

[17] K. Hu, C. Chen, Y. Zhu, G. Zeng, B. Huang, W. Chen, S. Liu, C. Lei, B. Li, Y. Yang, Ternary Z-scheme heterojunction of Bi_2WO_6 with reduced graphene oxide (rGO) and meso-tetra (4-carboxyphenyl) porphyrin (TCPP) for enhanced visible-light photocatalysis, J. Colloid. Interface Sci., 540 (2019) 115-125.

[18] W. Zhang, S. Gao, D. Chen, Preparation of Ce^{3+} doped Bi_2O_3 hollow needle-shape with enhanced visible-light photocatalytic activity, J. Rare Earths, 37 (2019) 726-731.

[19] Y. Chen, Q. Wu, L. Liu, J. Wang, Y. Song, The fabrication of self-floating Ti^{3+}/N co-doped TiO_2/diatomite granule catalyst with enhanced photocatalytic performance under visible light irradiation, Appl. Surf. Sci., 467-468 (2019) 514-525.

[20] S. Bao, H. Liang, C. Li, J. Bai, A heterostructure BiOCl nanosheets/TiO_2 hollow-tubes composite for visible light-driven efficient photodegradation antibiotic, J. Photochem. Photobiol., A, 397 (2020) 112590.

[21] J. Kang, C. Jin, Z. Li, M. Wang, Z. Chen, Y. Wang, Dual Z-scheme MoS_2/g-C_3N_4/Bi24O31Cl10 ternary heterojunction photocatalysts for enhanced visible-light photodegradation of antibiotic, J. Alloy. Compd., 825 (2020) 153975.

[22] J. Tian, L. Wei, Z. Ren, J. Lu, J. Ma, The facile fabrication of Z-scheme Bi_2WO_6-P25 heterojunction with enhanced photodegradation of antibiotics under visible light, J. Environ. Chem. Eng., 9 (2021) 106167.

[23] Z. Chen, X. Chu, X. Huang, H. Sun, L. Chen, F. Guo, Fabrication of visible-light driven CoP/$ZnSnO_3$ composite photocatalyst for high-efficient photodegradation of antibiotic pollutant, Sep. Purif. Technol., 257 (2021) 117900.

[24] J.T. Wang, Y.L. Cai, X.J. Liu, X.D. Zhang, F.Y. Cai, H.L. Cao, Z. Zhong, Y.F. Li, L. Lü, Unveiling the visible-light-driven photodegradation pathway and products toxicity of tetracycline in the system of Pt/$BiVO_4$ nanosheets, J. Hazard. Mater., 424 (2021) 127596.

[25] K. Sekar, C. Chuaicham, U. Balijapalli, W. Li, K. Wilson, A. F. Lee, K. Sasaki, Surfactant- and template-free hydrothermal assembly of Cu_2O visible light photocatalysts for trimethoprim degradation, Appl. Catal. B, 284 (2021) 119741.

[26] Z. Wei, J. Liu, W. Fang, M. Xu, Z. Qin, Z. Jiang, W. Shangguan, Photocatalytic hydrogen evolution with simultaneous antibiotic wastewater degradation via the visible-light-responsive bismuth spheres-g-C_3N_4 nanohybrid: Waste to energy insight, Chem. Eng. J., 358 (2019) 944-954.

[27] M. Salimi, M. Behbahani, H.R. Sobhi, M. Gholami, A. Jonidi Jafari, R. Rezaei

Kalantary, M. Farzadkia, A. Esrafili, A new nano-photocatalyst based on Pt and Bi co-doped TiO_2 for efficient visible-light photo degradation of amoxicillin, New J. Chem., 43 (2019) 1562-1568.

[28] M. Dou, J. Wang, B. Gao, C. Xu, F. Yang, Photocatalytic difference of amoxicillin and cefotaxime under visible light by mesoporous g-C_3N_4: Mechanism, degradation pathway and DFT calculation, Chem. Eng. J., 383 (2020) 123134.

[29] P.Y.Y. E.T. Wahyuni, N.H. Aprilita, Enhancement of visible-light photocatalytic activity of Cu-doped TiO_2 for photodegradation of amoxicillin in water, j. environ. Mater.Sci., 11 (2020) 670-683.

[30] F. Beshkar, A. Al-Nayili, O. Amiri, M. Salavati-Niasari, M. Mousavi-Kamazani, Visible light-induced degradation of amoxicillin antibiotic by novel CuI/$FePO_4$ p-n heterojunction photocatalyst and photodegradation mechanism, J. Alloy. Compd., 892 (2022) 162176.

[31] Y. Wang, G. Zuo, J. Kong, Y. Guo, Z. Xian, Y. Dai, J. Wang, T. Gong, C. Sun, Q. Xian, Sheet-on-sheet TiO_2/Bi_2MoO_6 heterostructure for enhanced photocatalytic amoxicillin degradation, J. Hazard. Mater., 421 (2022) 126634.

[32] S. Sohrabnezhad, A. Pourahmad, M.F. Karimi, Magnetite-metal organic framework core@shell for degradation of ampicillin antibiotic in aqueous solution, J. Solid State Chem., 288 (2020) 121420.

[33] W. Yang, Y. Wang, Enhanced electron and mass transfer flow-through cell with C_3N_4-MoS_2 supported on three-dimensional graphene photoanode for the removal of antibiotic and antibacterial potencies in ampicillin wastewater, Appl. Catal. B, 282 (2021) 119574.

[34] K. Wang, Y. Li, G. Zhang, J. Li, X. Wu, 0D Bi nanodots/2D Bi_3NbO_7 nanosheets heterojunctions for efficient visible light photocatalytic degradation of antibiotics: Enhanced molecular oxygen activation and mechanism insight, Appl. Catal. B, 240 (2019) 39-49.

[35] Y. Xu, Y. Ma, H. Ji, S. Huang, M. Xie, Y. Zhao, H. Xu, H. Li, Enhanced long-wavelength light utilization with polyaniline/bismuth-rich bismuth oxyhalide composite towards photocatalytic degradation of antibiotics, J. Colloid. Interface Sci., 537 (2019) 101-111.

[36] N. Zhang, X. Li, Y. Wang, B. Zhu, J. Yang, Fabrication of magnetically recoverable Fe_3O_4/CdS/g-C_3N_4 photocatalysts for effective degradation of ciprofloxacin under visible light, Ceram. Int., 46 (2020) 20974-20984.

[37] A.V. Karim, A. Shriwastav, Degradation of ciprofloxacin using photo, sono, and sonophotocatalytic oxidation with visible light and low-frequency ultrasound: Degradation kinetics and pathways, Chem. Eng. J., 392 (2020) 124853.

[38] J. Wang, L. Svoboda, Z. Němečková, M. Sgarzi, J. Henych, N. Licciardello, G. Cuniberti, Enhanced visible-light photodegradation of fluoroquinolone-based antibiotics and E. coli growth inhibition using Ag-TiO_2 nanoparticles, RSC Adv., 11 (2021) 13980-13991.

[39] A.S. Basaleh, A. Shawky, Z.I. Zaki, Visible light-driven photodegradation of

ciprofloxacin over sol-gel prepared Bi_2O_3-modified La-doped $NaTaO_3$ nanostructures, Ceram. Int., 47 (2021) 19205-19212.
[40] X.S. Nguyen, T.D. Pham, H.T. Vo, K.D. Ngo, Photocatalytic degradation of cephalexin by g-C_3N_4/Zn doped Fe_3O_4 under visible light, Environ. Technol., 42 (2021) 1292-1301.
[41] M. Aram, M. Farhadian, A.R. Solaimany Nazar, S. Tangestaninejad, P. Eskandari, B.-H. Jeon, Metronidazole and Cephalexin degradation by using of Urea/TiO_2/$ZnFe_2O_4$/Clinoptiloite catalyst under visible-light irradiation and ozone injection, J. Mol. Liq., 304 (2020) 112764.
[42] N. Askari, M. Beheshti, D. Mowla, M. Farhadian, Fabrication of $CuWO_4$/Bi_2S_3/ZIF67 MOF: A novel double Z-scheme ternary heterostructure for boosting visible-light photodegradation of antibiotics, Chemosphere, 251 (2020) 126453.
[43] S. Adhikari, H.H. Lee, D.-H. Kim, Efficient visible-light induced electron-transfer in z-scheme MoO_3/Ag/C_3N_4 for excellent photocatalytic removal of antibiotics of both ofloxacin and tetracycline, Chem. Eng. J., 391 (2020) 123504.
[44] S. Cipagauta-Díaz, A. Estrella-González, M. Navarrete-Magaña, R. Gómez, N doped-TiO_2 coupled to $BiVO_4$ with high performance in photodegradation of Ofloxacin antibiotic and Rhodamine B dye under visible light, Catal. Today, (2021).
[45] X. Chen, M. Zhang, H. Qin, J. Zhou, Q. Shen, K. Wang, W. Chen, M. Liu, N. Li, Synergy effect between adsorption and heterogeneous photo-Fenton-like catalysis on $LaFeO_3$/lignin-biochar composites for high efficiency degradation of ofloxacin under visible light, Sep. Purif. Technol., 280 (2022) 119751.
[46] X. Xie, S. Li, H. Zhang, Z. Wang, H. Huang, Promoting charge separation of biochar-based Zn-TiO_2/pBC in the presence of ZnO for efficient sulfamethoxazole photodegradation under visible light irradiation, Sci. Total Environ., 659 (2019) 529-539.
[47] R. Jiang, D. Wu, G. Lu, Z. Yan, J. Liu, R. Zhou, M. Nkoom, Fabrication of Fe_3O_4 quantum dots modified BiOCl/$BiVO_4$ p-n heterojunction to enhance photocatalytic activity for removing broad-spectrum antibiotics under visible light, J. Taiwan Inst. Chem. Eng., 96 (2019) 681-690.
[48] K. Arora, S. Karthikeyan, B.A. Shiekh, M. Kaur, H. Singh, G.R. Bhadu, T.S. Kang, In situ preparation of a nanocomposite comprising graphene and α-Fe_2O_3 nanospindles for the photo-degradation of antibiotics under visible light, New J. Chem., 44 (2020) 15567-15573.
[49] A. Kumar, S.K. Sharma, G. Sharma, C. Guo, D.N. Vo, J. Iqbal, M. Naushad, F.J. Stadler, Silicate glass matrix@Cu_2O/$Cu_2V_2O_7$ p-n heterojunction for enhanced visible light photo-degradation of sulfamethoxazole: High charge separation and interfacial transfer, J. Hazard. Mater., 402 (2021) 123790.
[50] C. Liu, J. Xu, X. Du, Q. Li, Y. Fu, M. Chen, Synthesis of Ag_2O-$KNbO_3$ heterojunction photocatalysts with enhanced visible-light-responsive

photocatalytic performance for sulfamethoxazole degradation, Opt. Mater., 112 (2021) 110742.